# Spin tunnel field-effect transistors based on two-dimensional van der Waals heterostructures

Shengwei Jiang<sup>1,2</sup>, Lizhong Li<sup>2</sup>, Zefang Wang<sup>2,3</sup>, Jie Shan<sup>1,2,4\*</sup>, and Kin Fai Mak<sup>1,2,4\*</sup>

<sup>1</sup>Laboratory of Atomic and Solid State Physics, Cornell University, Ithaca, NY, USA <sup>2</sup>School of Applied and Engineering Physics, Cornell University, Ithaca, NY, USA <sup>3</sup>Department of Physics, Penn State University, University Park, PA, USA <sup>4</sup>Kavli Institute at Cornell for Nanoscale Science, Ithaca, NY, USA

\*Emails: jie.shan@cornell.edu; kinfai.mak@cornell.edu.

#### **One-sentence summary**

A tunnel field-effect transistor with spin-dependent outputs that are voltage controllable and reversible can be created using a dual-gated graphene/CrI<sub>3</sub>/graphene tunnel junction.

A transistor based on spin rather than charge – a spin transistor – could potentially offer non-volatile data storage and improved performance compared with traditional transistors. Many approaches have been explored to realize spin transistors, but their development remains a considerable challenge. The recent discovery of two-dimensional magnetic insulators such as chromium triiodide (CrI<sub>3</sub>), which offer electrically switchable magnetic order and an effective spin filtering effect, can provide new operating principles for spin transistors. Here we report spin tunnel field-effect transistors (TFETs) based on dual-gated graphene/CrI<sub>3</sub>/graphene tunnel junctions. The devices exhibit an ambipolar behaviour and tunnel conductance that is dependent on the magnetic order in the CrI<sub>3</sub> tunnel barrier. The gate voltage switches the tunnel barrier between an interlayer antiferromagnetic and ferromagnetic state under a constant magnetic bias near the spin-flip transition, thus effectively and reversibly altering the device between a low and a high conductance state with a large hysteresis. By electrically controlling the magnetization configurations instead of the spin current, our spin TFETs achieve a high-low conductance ratio approaching 400%, suggesting they could be of value in the development of non-volatile memory applications.

Spin field-effect transistors (FETs) were first proposed by Datta and Das in 1990 <sup>1</sup>. These spin-based devices promise non-volatile data storage, and faster and more energy-efficient performance than current transistors <sup>2-4</sup>. In order to build spin transistors, a variety of approaches have been explored, including recent demonstrations based on van der Waals heterostructures <sup>5,6</sup>. All of these devices rely on spin injection and detection at ferromagnetic contacts, and voltage control of spin current in a semiconductor channel. Such devices face significant challenges in achieving a large high–low conductance ratio due to inefficient spin injection and spin relaxation in the semiconductor channels <sup>7,8</sup>.

The discovery of two-dimensional (2D) magnetic crystals <sup>9-19</sup> has provided a unique platform to explore new spintronic device concepts with unprecedented

controllability. In particular, the layered magnetic insulator  $CrI_3$  <sup>20</sup> exhibits an intriguing layer thickness-dependent magnetic order <sup>9</sup>: monolayer  $CrI_3$  is a ferromagnet with spins pointing out-of-plane, whereas bilayer  $CrI_3$  is an antiferromagnet consisting of two ferromagnetic monolayers with antiparallel spins. Under a magnetic field of less than 1 T, bilayer  $CrI_3$  can be turned into a ferromagnet through a spin-flip transition. Because of the relatively weak interlayer interaction, recent experiments have demonstrated antiferromagnet–ferromagnet switching in bilayer  $CrI_3$  by either a pure electric field <sup>21</sup> or electrostatic doping <sup>22,23</sup> under a constant magnetic bias.

In this Article, we report the development of a tunnel field-effect transistor (TFET) with spin-dependent outputs that are voltage controllable and reversible, by incorporating bilayer CrI<sub>3</sub> into a TFET as a magnetic tunnel barrier. In contrast to conventional spin transistors, these devices rely on the spin filtering effect <sup>24-27</sup> to inject and detect spin, and electrical switching of the magnetization configurations <sup>21-23</sup> in the tunnel barrier, rather than electrical control of spin current in the channel, to control the transistor outputs. The devices offer a large high–low conductance ratio approaching 400%.

## Graphene/CrI<sub>3</sub>/graphene tunnel field-effect transistor

Our device consists of a graphene/CrI<sub>3</sub>/graphene vertical junction with top and bottom gates (Fig. 1a). The two nearly symmetric gates are made of few-layer graphite gate electrodes and hexagonal boron nitride (hBN) gate dielectrics of ~ 20 nm. (See Methods for fabrication details and Supplementary Sections 1 and 2 for basic materials and device characterization.) Few-layer CrI<sub>3</sub> ranging from 2 to 4 layers has been investigated as a magnetic tunnel barrier. Figure 1a shows the simple case of a bilayer CrI<sub>3</sub> barrier with two magnetization configurations: two antiferromagnetically coupled monolayers (left) and ferromagnetically coupled monolayers (right). In most devices bilaver graphene with an appreciable band gap instead of gapless monolayer graphene has been chosen as both the source and drain contacts to achieve an ambipolar transistor as we demonstrate below. The gates can tune the Fermi level of the nearest graphene contact effectively, which modulates the conductance of the graphene/CrI<sub>3</sub>/graphene vertical junction through resonant tunneling <sup>28,29</sup>. More importantly, the gates can also induce a spin-flip transition in CrI<sub>3</sub> <sup>21-23</sup>, which causes a significant modulation in the tunnel conductance by the spin filtering effect. The spin filtering effect has been recently demonstrated in the form of large tunnel magnetoresistance (TMR) in tunnel junctions consisting of 2D CrI<sub>3</sub>  $^{24-27}$ . For instance, a change in the tunnel resistance by  $\sim 100\%$  has been reported when bilayer CrI<sub>3</sub> undergoes the spin-flip transition.

Figure 1b is the tunnel conductance G of a bilayer graphene/bilayer  $CrI_3$ /bilayer graphene junction measured under a small bias ( $V_b = 4 \text{ mV}$ ) as a function of top gate voltage  $V_{tg}$ . The back-gate voltage and magnetic field were kept at zero, and the sample temperature, at 4 K. Measurements at varying temperatures are included in Supplementary Sect. 3. An ambipolar behavior with a zero conductance (*i.e.* off) state is observed. This indicates a sizable band gap in both bilayer graphene contacts, which is confirmed by a direct in-plane transport measurement on the graphene contact (Supplementary Fig. S6). In contrast, no off state is observed when gapless monolayer

graphene is used as contacts (Supplementary Fig. S9). The band gap in bilayer graphene <sup>30,31</sup> is opened likely by a built-in interfacial electric field from the asymmetric hBN/bilayer graphene/CrI<sub>3</sub> structure. A detailed bias dependence measurement, combined with modeling of resonant tunneling in the junction, shows that the gap is around 100 meV (see Supplementary Sect. 5). Figure 1b also shows that both bilayer graphene contacts are unintentionally *p*-doped likely due to charge transfer to CrI<sub>3</sub>. Since the top gate is effectively screened by the top graphene contact and the CrI<sub>3</sub> barrier, its effect on the bottom graphene contact is negligible. Similarly, the effect of the bottom gate on the top graphene contact is also negligible (Supplementary Fig. S3 and S6). Below we study the basic operation of our TFET by focusing on one gate (the top gate) and the bilayer graphene/bilayer CrI<sub>3</sub>/bilayer graphene junction. The behavior of devices with thicker CrI<sub>3</sub> is similar (Supplementary Sect. 7).

The gate dependence of the tunnel conductance shows three distinct regions: p-p, p-i and p-n from left to right in Fig. 1b. Here the doping type of the graphene contacts is given in the order from the bottom layer to the top layer. The insets illustrate the band alignments of the two contacts and the tunnel barrier. Since only the top gate voltage is swept, the Fermi level in the bottom contact (left) is fixed inside the valence band; and the Fermi level in the top contact (right) is moved across the gap. In the zero-bias limit, the two Fermi levels are aligned. Under forward (backward) biasing by  $V_b$ , the Fermi level of the bottom contact is down (up) shifted by  $eV_b$  in our setup (insets of Fig. 1c-e). In the p-i region, the tunnel junction is off since the Fermi level of the top contact falls inside its energy gap and no state is available for resonant tunneling in the zero-bias limit. In the p-n region, we observe the characteristic negative differential conductance under forward biasing (dip 1 in Fig. 1c)  $^{28,29,32}$ . In the p-p region, there is a dip (which remains positive) in the differential conductance on each side of zero bias (Fig. 1d). Dip 3 depends on gate voltage much more strongly than dip 2. The dip positions are a good measure of the Fermi level in the graphene contacts. Their dispersion with  $V_{tq}$  is summarized in Fig. 1f (symbols), which is in good agreement with the resonant tunneling model (solid lines, for details see Supplementary Sect. 5). We note that the behavior of dip 2 and 3 is switched when the bottom gate voltage  $V_{bg}$  instead of the top gate voltage  $V_{ta}$  is applied (Fig. 1e), verifying that the two gates are symmetric.

## Spin-dependent transistor outputs

Next, we show that the TFET output depends on the magnetization configurations. Figure 2a - 2d are the magnetic-field dependence of the device conductance G for several representative gate voltages. In all cases, G exhibits a sharp jump around 0.5 T, which is correlated with the spin-flip transition in bilayer  $CrI_3$  (See Supplementary Fig. S4 for independent verification by magnetic circular dichroism). The magnetic hysteresis reflects the first-order nature of the spin-flip transition  $^{33}$ . We calculate  $TMR = \frac{G_{FM} - G_{AFM}}{G_{AFM}}$  using the conductance for the tunnel barrier in the antiferromagnetic ( $G_{AFM}$ ) and the ferromagnetic ( $G_{FM}$ ) states. In the p-p (Fig. 2a) and p-n region (Fig. 2d), the value is  $\sim 80\%$ . The TMR here is governed by the spin filtering efficiency of  $CrI_3$ . We estimate the spin filtering efficiency of each layer of  $CrI_3$  (the ratio of the transmission probability of electrons with spins parallel to antiparallel to the

We further perform systematic bias dependence measurements of the differential conductance of our TFET under varying magnetic fields to understand the origin of the observed shift between the gate dependence of  $G_{AFM}$  and  $G_{FM}$ . Figure 3a and 3b are the result for a representative p-n and p-p junction, respectively. We record the magnetic-field dependence of the position of dip 1 - 3 in Fig. 3c - 3e, respectively. The position of the negative differential conductance (dip 1, Fig. 3c) exhibits a clear upshift upon the spin-flip transition to the ferromagnetic state. This is consistent with a downshift of the Fermi level, or equivalently, extra hole doping in the graphene contacts (inset of Fig. 1c). The same conclusion can be reached from the analysis of the result of the p-p junction (Fig. 3b, 3d and 3e, and insets of Fig. 1d). It is also supported by direct in-plane transport in the top graphene contact (See Supplementary Sect. 4 for details). A plausible mechanism for the Fermi level shift is a magnetic-order-dependent band structure in  $CrI_3$  This can change the built-in electric field as well as charge transfer at the graphene/ $CrI_3$  interfaces. Future theoretical studies with accurate band structure calculations are needed for a quantitative description of our observation.

### Spin tunnel field-effect transistor operation

Finally, we note that the spin-flip transition field depends on gate voltage (Fig. 2a - 2d)  $^{22,23}$ . We utilize this key property to realize the spin-TFET action, *i.e.* control the tunnel conductance G by electrically switching the magnetic order in the tunnel barrier. To minimize the trivial conductance change due to electrostatic doping, we choose a range of gate voltage from the p-p region ( $V_{tg} < 0$  V), where G is weakly gate dependent in the absence of magnetism. Figure 4a shows the gate dependence of G under a constant magnetic bias (0.76 T). This field is slightly above the spin-flip transition of bilayer  $CrI_3$  under  $V_{tg} = 0$  V. The gate voltage can repeatedly alter the TFET between a high and a low conductance state (symbols). As a reference, we have also included the high and low conductance states that have been achieved under 0.92 T and 0.55 T with the  $CrI_3$  barrier in the ferromagnetic and antiferromagnetic state (dashed lines). A ratio of  $\sim 35\%$  in the tunnel conductance for the two magnetization configurations (Fig. 1a) has been achieved through gating which also shows a large hysteresis in gate voltage. The conductance ratio between different magnetization configurations can be significantly enhanced by using thicker tunnel barriers on the expense of the tunnel conductance. Figure 4b shows

the result for a device with 3-layer CrI<sub>3</sub> barrier under a constant magnetic bias of 1.7 T. Nearly 200% change in the tunnel conductance is achieved. Moreover, nearly 400% is achieved in a TFET with 4-layer CrI<sub>3</sub> barrier under a constant magnetic bias of 1.77 T (Fig. 4c). (See Supplementary Sect. 7 for detailed characterizations of 3-layer and 4-layer CrI<sub>3</sub> devices). As the number of layers in CrI<sub>3</sub> increases, each layer acts as an additional spin filter in series, thus greatly enhancing the conductance ratio between different magnetization configurations. However, the doping efficiency and thus the effectiveness of voltage control of the magnetic order also decrease substantially, and the spin transistor action becomes harder to achieve.

#### **Conclusions**

By combining electrically-controlled interlayer magnetic order for "writing" and a spin filtering effect for "reading" in a single device, we have created a TFET with spin-dependent outputs that are voltage controllable and reversible. Although the current device, which is based on dual-gated graphene–CrI<sub>3</sub> heterostructures, requires a relatively large bias magnetic field and low temperature for operation, the device concept is applicable to a wide range of materials, some of which could potentially overcome these limitations. For example, artificial layered antiferromagnets <sup>35</sup> with similar spin-flip behaviors, but higher critical temperatures, could potentially replace CrI<sub>3</sub> for operation at elevated temperatures. The bias magnetic field could be significantly reduced or eliminated through more efficient gating or the exchange bias effect. Our device concept could thus provide a new approach for exploring non-volatile and reconfigurable memory and logic applications <sup>36</sup>.

#### Methods

**Device fabrication.** Van der Waals heterostructures of CrI<sub>3</sub>, hexagonal boron nitride (hBN) and graphene were fabricated by the layer-by-layer dry transfer method <sup>37</sup>. Images of sample devices are shown in Supplementary Fig. S1. In this process, atomically thin samples of CrI<sub>3</sub>, hBN and graphene were first exfoliated from their bulk crystals (HQ graphene) onto silicon substrates covered with a 300-nm thermal oxide layer. thickness of thin flakes was initially estimated from their optical reflectance contrast on silicon substrates. The thickness of CrI<sub>3</sub> was verified by the magnetization measurement under an out-of-plane magnetic field (Supplementary Fig. S2) using magnetic circular dichroism as described below. The thickness of hBN flakes was determined by atomic force microscopy, and of monolayer and bilayer graphene, by Raman spectroscopy. The selected thin flakes of appropriate thickness and geometry were then picked up one-byone by a stamp consisting of a thin layer of polycarbonate (PC) on polydimethylsiloxane (PDMS). The complete stack was then deposited onto substrates with pre-patterned Au electrodes. The residual PC on the device surface was dissolved in chloroform before measurements. Since atomically thin CrI<sub>3</sub> is extremely air sensitive, it was handled in a nitrogen gas environment with less than one-part-per-million oxygen and moisture inside a glovebox and was removed from the glovebox only after being fully encapsulated.

**Electrical characterization.** The device characterization was carried out in an Attocube closed-cycle cryostat (attoDry1000) down to 4 K. The tunnel conductance of the

graphene/CrI<sub>3</sub> tunnel junctions was measured by biasing CrI<sub>3</sub> using graphene source and drain contacts (Fig. 1a). The bias voltage was kept in the low bias regime (4 mV in amplitude). For the magnetic field and gate voltage dependence studies of the tunnel conductance, the bias was modulated at a relatively low frequency (~ 17 Hz) and the resultant current was measured with a lock-in amplifier to reduce noise. The tunnel conductance was calculated as the ratio of current to bias. The bias dependence of the tunnel current was studied by applying a dc bias voltage using a sourcemeter and measuring the resultant dc current using a current preamplifier. The differential conductance as a function of bias voltage was obtained via numerical differentiation of the bias dependence of the tunnel current.

**Magnetic circular dichroism.** The magnetization of  $CrI_3$  was characterized by magnetic circular dichroism (MCD) using a HeNe laser at 633 nm. An objective of numerical aperture 0.8 was used to focus the excitation beam to a sub-micron spot size on the devices. The optical power on the devices was limited to 5  $\mu$ W. The reflected light from the devices was collected by the same objective and detected by a photodiode. The helicity of the optical excitation was modulated between left and right by a photoelastic modulator at 50.1 kHz. The MCD was determined as the ratio of the ac component (measured by a lock-in amplifier) to the dc component (measured by a multimeter) of the reflected light intensity.

### **Data availability**

The data supporting the plots within this paper and other findings of this study are available from the corresponding authors upon request.

#### References

- Datta, S. & Das, B. Electronic analog of the electro optic modulator. *Applied Physics Letters* **56**, 665-667 (1990).
- Žutić, I., Fabian, J. & Das Sarma, S. Spintronics: Fundamentals and applications. *Reviews of Modern Physics* **76**, 323-410 (2004).
- 3 Awschalom, D. D. & Flatté, M. E. Challenges for semiconductor spintronics. *Nature Physics* **3**, 153 (2007).
- Sugahara, S. & Nitta, J. Spin-Transistor Electronics: An Overview and Outlook. *Proceedings of the IEEE* **98**, 2124-2154 (2010).
- 5 Yan, W. et al. A two-dimensional spin field-effect switch. *Nature Communications* 7, 13372 (2016).
- Dankert, A. & Dash, S. P. Electrical gate control of spin current in van der Waals heterostructures at room temperature. *Nature Communications* **8**, 16093 (2017).
- 7 Koo, H. C. *et al.* Control of Spin Precession in a Spin-Injected Field Effect Transistor. *Science* **325**, 1515 (2009).
- 8 Chuang, P. *et al.* All-electric all-semiconductor spin field-effect transistors. *Nature Nanotechnology* **10**, 35 (2014).
- 9 Huang, B. *et al.* Layer-dependent ferromagnetism in a van der Waals crystal down to the monolayer limit. *Nature* **546**, 270 (2017).

- Gong, C. *et al.* Discovery of intrinsic ferromagnetism in two-dimensional van der Waals crystals. *Nature* **546**, 265 (2017).
- Yao, T., Mason, J. G., Huiwen, J., Cava, R. J. & Kenneth, S. B. Magneto-elastic coupling in a potential ferromagnetic 2D atomic crystal. *2D Materials* **3**, 025035 (2016).
- Lee, J.-U. *et al.* Ising-Type Magnetic Ordering in Atomically Thin FePS3. *Nano Lett* **16**, 7433-7438 (2016).
- Bonilla, M. *et al.* Strong room-temperature ferromagnetism in VSe2 monolayers on van der Waals substrates. *Nature Nanotechnology* **13**, 289-293 (2018).
- O'Hara, D. J. et al. Room Temperature Intrinsic Ferromagnetism in Epitaxial Manganese Selenide Films in the Monolayer Limit. Nano Lett 18, 3125-3131 (2018).
- Du, K.-z. *et al.* Weak Van der Waals Stacking, Wide-Range Band Gap, and Raman Study on Ultrathin Layers of Metal Phosphorus Trichalcogenides. *ACS Nano* **10**, 1738-1743 (2016).
- Zhou, B. *et al.* Possible structural transformation and enhanced magnetic fluctuations in exfoliated α-RuCl3. *Journal of Physics and Chemistry of Solids* (2018).
- Wang, Z. *et al.* Electric-field control of magnetism in a few-layered van der Waals ferromagnetic semiconductor. *Nature Nanotechnology* **13**, 554-559 (2018).
- Deng, Y. J. *et al.* Gate-tunable room-temperature ferromagnetism in two-dimensional Fe3GeTe2. *Nature* **563**, 94 (2018).
- Ghazaryan, D. *et al.* Magnon-assisted tunnelling in van der Waals heterostructures based on CrBr3. *Nature Electronics* **1**, 344-349 (2018).
- McGuire, M. A. Crystal and Magnetic Structures in Layered, Transition Metal Dihalides and Trihalides. *Crystals* 7, 121 (2017).
- Jiang, S., Shan, J. & Mak, K. F. Electric-field switching of two-dimensional van der Waals magnets. *Nature Materials* **17**, 406-410 (2018).
- Jiang, S., Li, L., Wang, Z., Mak, K. F. & Shan, J. Controlling magnetism in 2D CrI3 by electrostatic doping. *Nature Nanotechnology* **13**, 549-553 (2018).
- Huang, B. *et al.* Electrical control of 2D magnetism in bilayer CrI3. *Nature Nanotechnology* **13**, 544-548 (2018).
- Song, T. *et al.* Giant tunneling magnetoresistance in spin-filter van der Waals heterostructures. *Science* **360**, 1214-1218 (2018).
- Klein, D. R. *et al.* Probing magnetism in 2D van der Waals crystalline insulators via electron tunneling. *Science* **360**, 1218-1222 (2018).
- Wang, Z. et al. Very large tunneling magnetoresistance in layered magnetic semiconductor CrI3. *Nature Communications* **9**, 2516 (2018).
- Kim, H. H. *et al.* One Million Percent Tunnel Magnetoresistance in a Magnetic van der Waals Heterostructure. *Nano Lett* **18**, 4885-4890 (2018).
- Britnell, L. *et al.* Field-Effect Tunneling Transistor Based on Vertical Graphene Heterostructures. *Science* **335**, 947 (2012).
- Britnell, L. *et al.* Resonant tunnelling and negative differential conductance in graphene transistors. *Nature Communications* **4**, 1794 (2013).
- Zhang, Y. *et al.* Direct observation of a widely tunable bandgap in bilayer graphene. *Nature* **459**, 820 (2009).

- McCann, E. Asymmetry gap in the electronic band structure of bilayer graphene. *Physical Review B* **74**, 161403 (2006).
- Esaki, L. New Phenomenon in Narrow Germanium p-n Junctions. *Physical Review* **109**, 603-604 (1958).
- 33 Stryjewski, E. & Giordano, N. Metamagnetism. *Advances in Physics* **26**, 487-650 (1977).
- Jiang, P., Li, L., Liao, Z., Zhao, Y. X. & Zhong, Z. Spin Direction-Controlled Electronic Band Structure in Two-Dimensional Ferromagnetic CrI3. *Nano Lett* **18**, 3844-3849 (2018).
- 35 Chen, B. *et al.* All-oxide–based synthetic antiferromagnets exhibiting layer-resolved magnetization reversal. *Science* **357**, 191 (2017).
- Matsukura, F., Tokura, Y. & Ohno, H. Control of magnetism by electric fields. *Nature Nanotechnology* **10**, 209 (2015).
- Wang, L. *et al.* One-Dimensional Electrical Contact to a Two-Dimensional Material. *Science* **342**, 614 (2013).

#### Acknowledgements

The research was supported by the National Science Foundation (NSF) under award DMR-1807810 for the sample and device fabrication, the Office of Naval Research (ONR) under award N00014-18-1-2368 for the device characterization, and the Air Force Office of Scientific Research (AFOSR) Hybrid Materials MURI under award FA9550-18-1-0480 for optical measurements. This work was also partially supported by the Cornell Center for Materials Research with funding from the NSF MRSEC program (DMR-1719875) for the low-temperature studies. It was performed in part at Cornell NanoScale Facility, an NNCI member supported by NSF Grant NNCI-1542081.

#### **Author contributions**

S.J., J.S., and K.F.M. designed the study and co-wrote the manuscript. S.J. performed the bulk of the measurements and data analysis. L.L and Z.W. contributed to the sample and device fabrication. All authors discussed the results and commented on the manuscript.

### **Competing interests**

The authors declare no competing financial interests.

## **Figures**

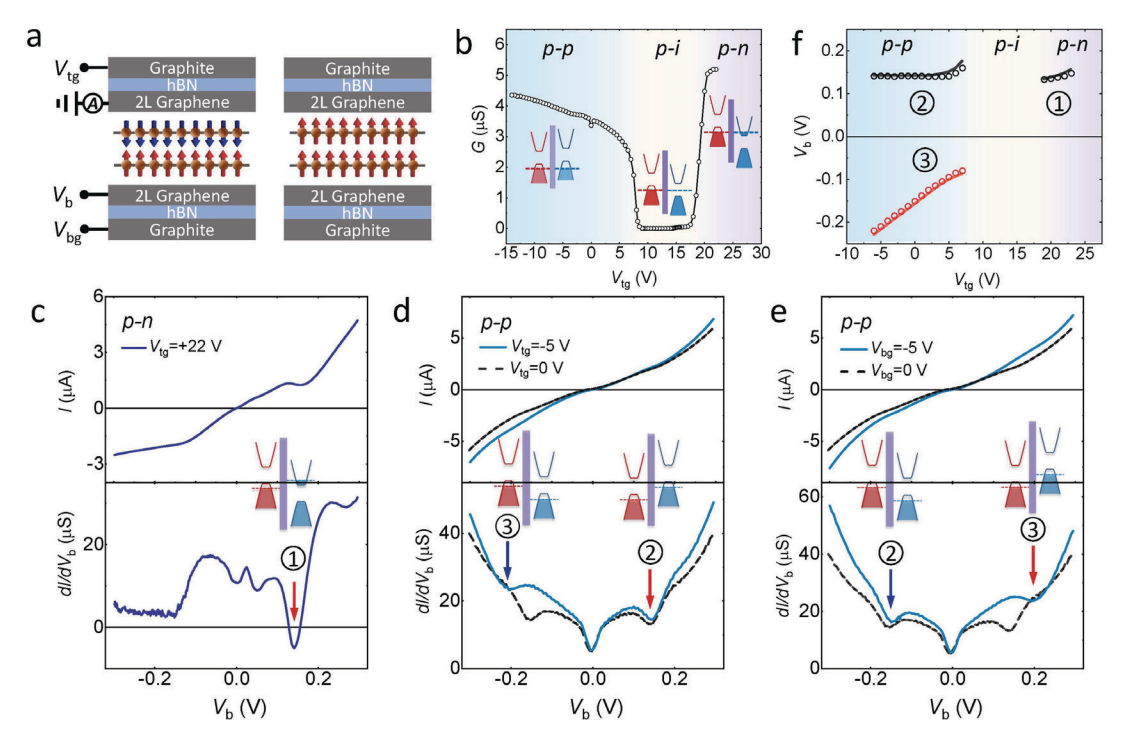


**Figure 1** | **Tunnel field-effect transistor (TFET) based on graphene/CrI<sub>3</sub> heterostructures. a**, Operational principle of a spin-TFET based on gate-controlled spin-flip transition in bilayer CrI<sub>3</sub> and spin filtering in the tunnel junction. Arrows indicate the spin orientation in CrI<sub>3</sub> layers. The left and right panels correspond to a low and a high tunnel conductance state, respectively. **b**, Gate dependence of tunnel conductance shows *p-p*, *p-i* and *p-n* regions for device 1. The feature at zero gate voltage is due to the resistance of the graphene contact in series with the tunnel junction. **c**, **d**, Bias dependence of tunnel current (upper panel) and differential conductance (lower panel) for representative *p-n* (**c**) and *p-p* (**d**) junctions. **e**, Same as **d** under the bottom instead of the top gate voltage. **f**, Gate dependence of bias voltages that correspond to differential conductance dip 1 - 3 as defined by arrows in **c** and **d**. Error bar is smaller than the data symbol. The insets in **b** - **e** show the band alignments of the bottom (red) and top (blue) bilayer graphene contacts and the CrI<sub>3</sub> barrier (purple). Shaded areas are filled states.

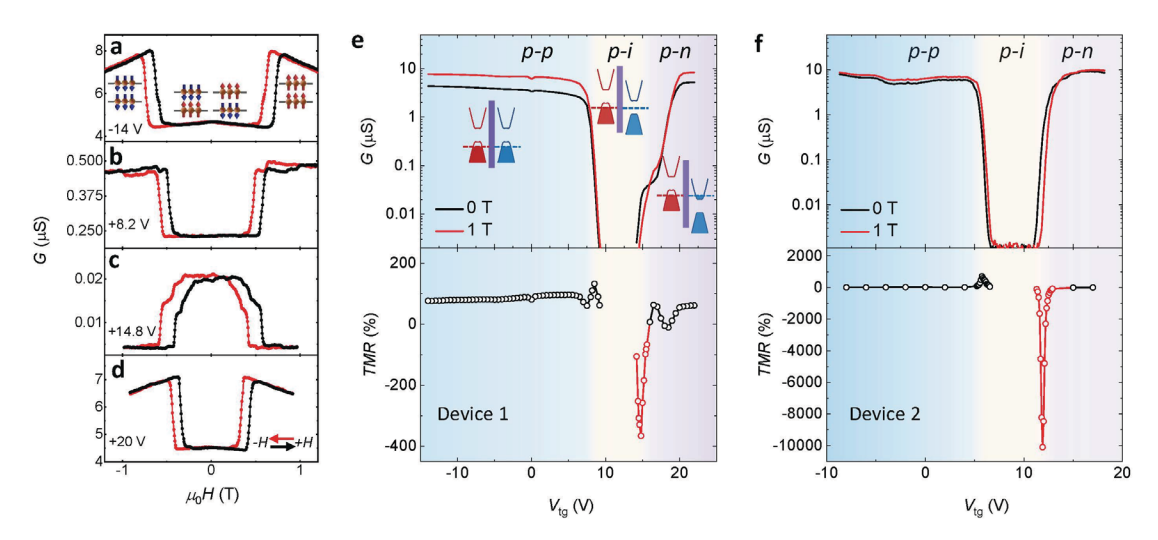
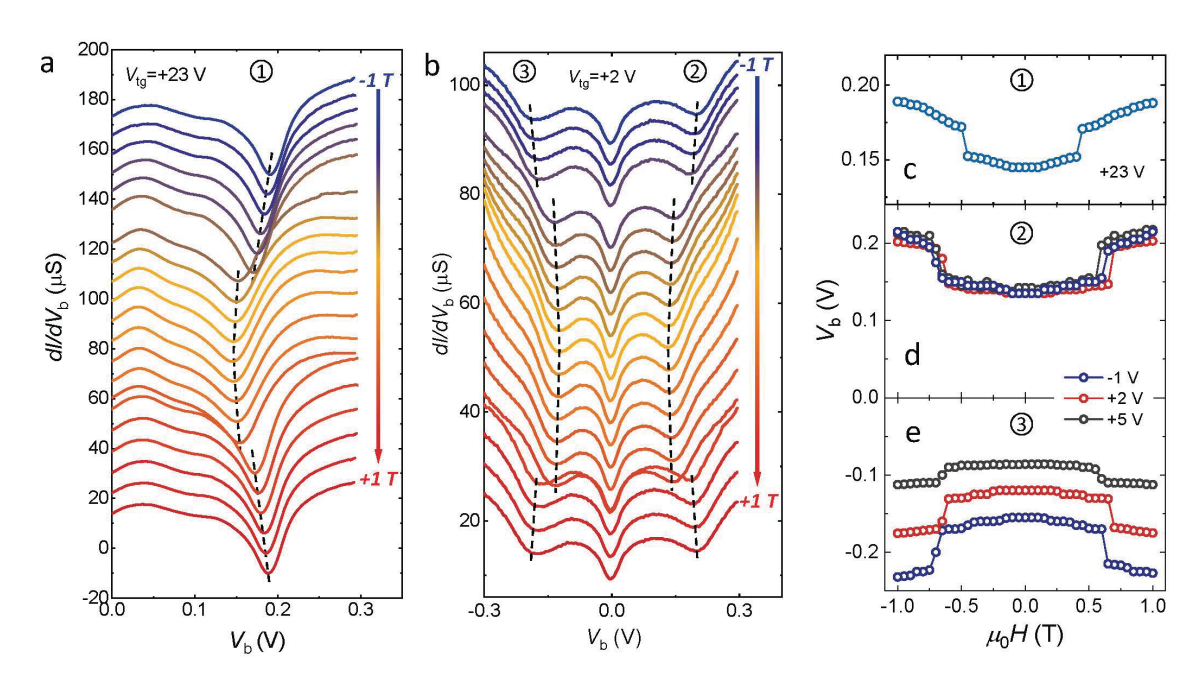
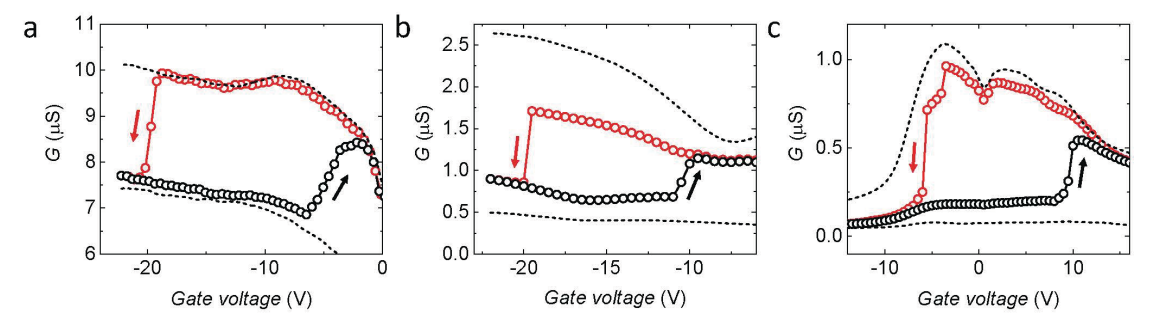


Figure 2 | Tunable tunnel magnetoresistance (TMR).  $\mathbf{a} - \mathbf{d}$ , Magnetic-field dependence of tunnel conductance at varying top gate voltages in the p-p ( $\mathbf{a}$ ), boundaries of p-i ( $\mathbf{b}$ ,  $\mathbf{c}$ ), and p-n ( $\mathbf{d}$ ) region.  $\mathbf{e}$ , Gate dependence of tunnel conductance under an out-of-plane magnetic field of 0 T and 1 T (upper panel), and TMR (lower panel) calculated from the measured magnetic-field dependence of tunnel resistance loops for device 1. The black and red symbols denote, respectively, the positive and negative values for TMR. The insets show the band alignments of the p-p, p-i and p-n tunnel junctions.  $\mathbf{f}$ , Same as  $\mathbf{e}$  for device 2. Error bar is smaller than the data symbol.



**Figure 3** | **Magnetic-transition-induced band shift. a**, **b**, Bias dependence of differential tunnel conductance of device 1 for a representative *p-n* (**a**) and *p-p* (**b**) junction. Results for magnetic field varying from 1 T to -1 T with a step size of 0.1 T are vertically displaced by the same amount for clarity. The dashed lines are guides to the eye for the evolution of differential conductance dip 1 (**a**) and dip 2 and 3 (**b**) as defined in Fig. 1c and 1d. **c** - **e**, Magnetic-field dependence of bias voltage corresponding to dip 1 (**c**), 2 (**d**) and 3 (**e**) for representative top gate voltages. The magnetic field was scanned from -1 T to 1 T. Error bar is smaller than the data symbol.



**Figure 4** | **Spin-TFET action. a**, Tunnel conductance of a TFET with a bilayer  $CrI_3$  tunnel barrier is repeatedly switched by gating under a constant magnetic bias of 0.76 T. The top and bottom gate voltages are identical and their sum is shown in the horizontal axis. Black and red symbols correspond to measurements while sweeping the gate voltage forward and backward, respectively. A change of  $\sim 35\%$  is seen in the tunnel conductance. The conductance at 0.55 T and 0.92 T is included as a reference in dashed lines. **b**, The same as in **a** for a TFET with a three-layer  $CrI_3$  tunnel barrier under a constant magnetic bias of 1.7 T. A change of  $\sim 200\%$  is seen in the tunnel conductance. **c**, The same as in **a** for a TFET with a four-layer  $CrI_3$  tunnel barrier under a constant magnetic bias of 1.77 T. A change of  $\sim 400\%$  is seen in the tunnel conductance.